

Alu RNA induces NLRP3 expression through TLR7 activation in α -1-antitrypsin-deficient macrophages

Jungnam Lee,¹ Naweed Mohammad,¹ Yuanqing Lu,¹ Keunsoo Kang,² Kyudong Han,^{2,3} and Mark Brantly¹

¹Division of Pulmonary, Critical Care and Sleep Medicine, University of Florida, Gainesville, Florida, USA. ²Department of Microbiology, Dankook University College of Natural Science, Cheonan, Republic of Korea. ³Center for Bio-Medical Engineering Core Facility, Dankook University, Cheonan, Republic of Korea.

α -1 antitrypsin (AAT) is a serine protease inhibitor that plays a pivotal role in maintaining lung homeostasis. The most common AAT allele associated with AAT deficiency (AATD) is PiZ. Z-AAT accumulates in cells due to misfolding, causing severe AATD. The major function of AAT is to neutralize neutrophil elastase in the lung. It is generally accepted that loss of antiprotease function is a major cause of COPD in individuals with AATD. However, it is now being recognized that the toxic gain-of-function effect of Z-AAT in macrophage likely contributes to lung disease. In the present study, we determined that TLR7 signaling is activated in Z-MDMs, and the expression level of NLRP3, one of the targets of TLR7 signaling, is significantly higher in Z- compared with M-MDMs. We also determined that the level of endosomal *Alu* RNA is significantly higher in Z-compared with M-MDMs. *Alu* RNA is a known endogenous ligand that activates TLR7 signaling. Z-AAT likely induces the expression of *Alu* elements in MDMs and accelerates monocyte death, leading to the higher level of endosomal *Alu* RNA in Z-MDMs. Taken together, this study identifies a mechanism responsible for the toxic gain of function of Z-AAT macrophages.

Introduction

α -1-Antitrypsin (AAT) is the most abundant serine protease inhibitor in human plasma and plays an important role in limiting lung injury triggered by proteases such as neutrophil elastase, proteinase 3, and cathepsin G (1, 2). The main function of AAT is to suppress proteolytic activities of serine proteases in the lower respiratory tract, protecting the alveolar matrix from destruction by these proteases. Besides antiprotease function, AAT also has antiinflammatory and immunomodulatory properties (3, 4). AAT is encoded by the SERine Protein INhibitor-A1 (*SERPINA1*) gene, and more than 500 single-nucleotide variants of the gene have been reported in mutation databases (5). Among them, the Z variant is associated with the most severe form of AAT deficiency, which is a hereditary disorder characterized by a low concentration of AAT. The Z-AAT variant differs from the WT, M-AAT, by a single glutamic acid to lysine substitution at position 342 (Glu342Lys) on the protein (6). This mutation in Z-AAT does not inhibit protein synthesis but causes defective secretion by modifying the structure of the protein (7). Due to the structural change, Z-AAT is misfolded and degraded, and it forms polymers within the cells, lowering the concentration of circulating AAT and causing inadequate antiprotease protection in the lower respiratory tract (8, 9).

AATD results in the imbalance between antiproteases and proteases and leads to the development of lung diseases such as emphysema (10, 11). The loss of antiprotease function has been focused on as the major cause of Z-AAT-associated lung diseases, while the retention and accumulation of misfolded Z-AAT have been studied in liver diseases such as liver cirrhosis and hepatocellular carcinoma (12–14). However, recent studies about Z-AAT found the toxic gain-of-function effect of intracellular Z-AAT not only in hepatocytes, but also in neutrophils, monocytes, and alveolar macrophages (15–17). It was previously demonstrated that Z-AAT accumulates in the endoplasmic reticulum (ER) of monocytes and leads to ER stress, which contributes to inflammatory phenotypes in ZZ monocytes exhibiting increased levels of inflammatory cytokines and activation of NF- κ B signaling (16). In addition, it was found that the misfolded Z-AAT protein accumulates within the ER of neutrophils, leading to the increased expression of CHOP,

Conflict of interest: The authors have declared that no conflict of interest exists.

Copyright: © 2022, Lee et al. This is an open access article published under the terms of the Creative Commons Attribution 4.0 International License.

Submitted: January 25, 2022

Accepted: April 29, 2022

Published: June 22, 2022

Reference information: *JCI Insight*. 2022;7(12):e158791.
<https://doi.org/10.1172/jci.insight.158791>.

an ER stress marker, and TNF- α , which accelerates the apoptosis of ZZ-neutrophils (15). A higher level of TNF- α was also reported in Z-MDMs where innate immune function was impaired (18). Altogether, substantial evidence supports that the accumulation of intracellular Z-AAT in macrophages likely plays a key role in Z-AAT-associated lung diseases.

Alveolar macrophages reside at the interface between air and lung tissue, serving as the front line of cellular defense against respiratory pathogens. The functional phenotypes of alveolar macrophages are determined in response to the microenvironment of the lung, and their functions are critical for lung homeostasis by clearing cell debris, pathogens, and oxidized surfactant; by resolving inflammation; and by repairing damaged tissue. Under some conditions, alveolar macrophages produce low levels of inflammatory cytokines and generally suppress inflammation (19). However, Z-AAT polymerizes and accumulates in alveolar macrophages, which induces the expression of inflammatory cytokines and subsequently promotes lung inflammation. The previous findings indicate that intracellular Z-AAT could be a direct or indirect cause of the activated inflammatory signaling in alveolar macrophages (17, 18). However, the molecular mechanism underlying Z-AAT-associated inflammation has not been studied. In this study, we conducted RNA-Seq of M- and Z-MDMs to identify molecular signaling, which triggers the activation of inflammatory signaling in Z-MDMs. The result found that TLR7 signaling is activated in Z-MDMs, and the expression level of NLRP3, one of end molecules of TLR7 signaling and a critical component of inflammasomes, is approximately 5 times higher in Z-MDMs than M-MDMs. TLR7 is a pivotal innate immune receptor that recognizes bacterial or viral single-stranded RNA. Therefore, TLR7 has important roles in viral or bacterial infections, but excessive TLR7 activation could disrupt lung homeostasis by causing sustained production of proinflammatory cytokines and chemokines. TLR7 is initially synthesized as a monomer, inactive form, in the ER, and properly folded TLR7 exits the ER as a monomer. TLR7 dimerizes upon ligand binding in the endosome and undergoes proteolytic cleavage for its functional maturation. The ligand binding sites of TLR7 are exposed to the endosomal lumen to prevent their binding to endogenous genomic materials (20, 21). However, there is accumulating evidence that endosomal TLR7 could be activated by endogenous ligands such as *Alu* elements (22, 23). Peripheral blood mononuclear cells (PBMCs) were previously transfected with *Alu*-containing plasmid, and the expression levels of inflammatory cytokines including TNF- α were highly increased in the transfected cells. But when the transfected cells were incubated with TLR7 antagonist, the expression levels of inflammatory cytokines were not increased by *Alu* elements. The result supports that *Alu* is an endogenous ligand to activate endosomal TLR7 signaling (22). Indeed, TLR7 activation by endogenous ligands has been implicated in the pathogenesis of autoimmune diseases (24). Interestingly, in this study, we found that the transcription rate of *Alu* elements is significantly higher in Z-MDMs than M-MDMs, and NF- κ B signaling is activated in Z-MDMs.

Taken together, this study demonstrates that Z-AAT promotes inflammatory signaling in macrophages and determines the underlying molecular mechanisms, the activation of TLR7, and NF- κ B signaling. Therefore, the findings from this study may translate to developing a targeted therapeutic strategy to suppress the activation of inflammatory signaling in alveolar macrophages and, therefore, reduce the burden of lung disease in AATD individuals.

Results

Transcriptional profiling of MDMs. RNA-Seq of 12 MDM samples generated 30 million reads per sample, of which over 95% mapped uniquely onto the human genome. RNA-Seq data were projected to a 2D plane spanned by their first 2 principal components to produce a principal component analysis (PCA) plot. PCA plot shows that M-MDMs and Z-MDMs are distinctly clustered (Figure 1A). When genes with an adjusted $P < 0.05$ and absolute \log_2 fold change > 1 were defined as differentially expressed genes (DEGs), 131 DEGs were identified between M-MDMs and Z-MDMs. Among them, 68 genes were upregulated, while 63 genes were downregulated in Z-MDMs. The DEGs are visualized by a volcano plot (Figure 1B). The lists of the top 30 upregulated genes and top 30 downregulated genes in Z-MDMs are shown in Supplemental Tables 1 and 2 (supplemental material available online with this article; <https://doi.org/10.1172/jci.insight.158791DS1>), respectively. IPA analysis of the DEGs created a treemap that visualizes the downstream function and disease of gene expression changes in Z-MDM (Figure 1C). The treemap analysis found that biological processes of the inflammatory response, chemotaxis, and immune cell movements are activated in Z-MDMs. Indeed, the result is consistent with the findings from previous studies about Z-AAT (18). Figure 1D depicts a network of the molecules that are involved in the biological processes activated in Z-MDMs. The molecular network analysis found that TNF- α signaling is activated in Z-MDMs.

TNF- α is known to inhibit macrophage efferocytosis of apoptotic neutrophils in a concentration-dependent manner (25), which could, at least in part, explain the accumulation of alveolar neutrophils in AATD individuals with a Z-AAT genotype. DEGs were clustered by their gene ontology, and the enrichment of gene ontology terms was tested using Fisher's exact test (GeneSCF v1.1-p2). Figure 2 shows gene ontology (GO) terms that are significantly enriched with an adjusted P value less than 0.05 in the DEGs. The main biofunctions related to the DEGs were chemokine-mediated signaling pathways, inflammatory responses, and neutrophil chemotaxis. We also examined the physical and functional interactions between proteins that are upregulated in Z-MDMs using STRING. The result shows interactions between molecules associated with the chemokine-mediated signaling pathway and molecules associated with regulation of acute inflammatory response (Supplemental Figure 1). We conducted the upstream regulator analysis of the DEGs using IPA software. The upstream regulator analysis tool analyzes linkage to DEGs through coordinated expression to identify potential upstream regulators, including transcription factors and any gene that has been observed experimentally to affect gene expression. The analysis found that TLR7, MYD88, and NF- κ B signaling are activated in Z-MDMs (Table 1). It is known that the activation of TLR7 recruits MYD88, which subsequently activates NF- κ B signaling (26).

Validation of RNA-Seq data using qPCR. The analysis of RNA-Seq data between M- and Z-MDMs found that neutrophil chemotaxis is activated in Z-MDMs. The accumulation of alveolar neutrophils is a hallmark of AAT-deficient individuals. RNA-Seq found that the expression levels of *CXCL1*, *CXCL5*, and *CXCL8* are significantly higher in Z-MDMs. The 3 cytokines are well-known neutrophil chemoattractant factors and neutrophil-related inflammatory mediators (27–29). Therefore, the higher expression levels of the cytokines in alveolar macrophages will lead to a higher migration rate of neutrophils to the pulmonary alveolus, increasing the number of alveolar neutrophils and enhancing neutrophil-related inflammation. Using quantitative PCR (qPCR), we compared the expression levels of *CXCL1*, *CXCL5*, and *CXCL8* between M-MDMs and Z-MDMs, and the result verified that the expression levels of the neutrophil chemoattractant factors are significantly higher in Z-MDMs than M-MDMs (Figure 3, A–C; $P < 0.05$). One of the DEGs between M-MDMs and Z-MDMs was *NLRP3*. The RNA-Seq data analysis found that the expression level of *NLRP3* is significantly higher in Z-MDMs than M-MDMs. *NLRP3* is expressed predominantly in macrophages and is an intracellular sensor that detects a broad range of microbial motifs, endogenous danger signals, and environmental irritants (30, 31). We also compared the expression level of *NLRP3* between M- and Z-MDMs using qPCR and verified the higher expression level of *NLRP3* in Z-MDMs (Figure 3D; $P = 0.026$). Through IPA analysis of the DEGs, we found that TLR7 signaling is activated in Z-MDMs, as described above. One of downstream molecules of TLR7 signaling is *NLRP3* (32). Based on the results, we suspected that TLR7 signaling is activated in Z-MDMs, leading to the increased expression of *NLRP3* in the cells.

Activation of TLR7 and NF- κ B in Z-MDMs. TLR7 is an endosomal innate immune sensor and is activated by binding to single-stranded RNAs. Unstimulated TLR7 is monomeric. In the presence of single-stranded RNA, TLR7 forms a dimer and undergoes activation following proteolytic cleavage. To determine whether TLR7 is activated in Z-MDMs, we isolated total proteins of MDM samples using nondenaturing lysis buffer and performed native polyacrylamide gel electrophoresis (PAGE) of the protein samples (Figure 4, A and B). Since the activation of TLR7 requires proteolytic cleavage, cleaved TLR7 is an indicator for TLR7 activation. The band intensities of cleaved TLR7 and full-length monomeric TLR7 were quantified using ImageJ (NIH). The ratio of cleaved TLR7 to full-length monomeric TLR7 was calculated in each MDM sample and compared between M- and Z-MDMs. The result shows that the level of activated TLR7 is significantly higher in Z-MDMs compared with M-MDMs (Figure 4C; $P = 0.0043$), supporting that TLR7 signaling is activated in Z-MDMs. NF- κ B is also a downstream molecule of activated TLR7 signaling. It was previously reported that NF- κ B signaling is activated in the cell with the Z-AAT genotype (33). NF- κ B activation is determined by measuring the levels of p50 and phosphorylated p65 in the cells. The IKK kinase complex is the core element of NF- κ B activation. Activated IKK β can phosphorylate p105, resulting in the degradation of p105 to generate p50 (34). p65 is one of the essential components that form the NF- κ B transcription factor complex. Phosphorylated p65 is another indicator for NF- κ B activation (35). To examine whether NF- κ B is activated in Z-MDMs, we compared the levels of p50 and phosphorylated p65 between M- and Z-MDMs. Figure 5, A–C, shows that the level of p50 is significantly higher in Z-MDMs than M-MDMs (Figure 5C; $P = 0.026$). In addition, Figure 5, D–F, shows that the level of phosphorylated p65 is significantly higher in Z-MDMs than M-MDMs (Figure 5F; $P = 0.0043$), indicating that NF- κ B signaling is activated in Z-MDMs.

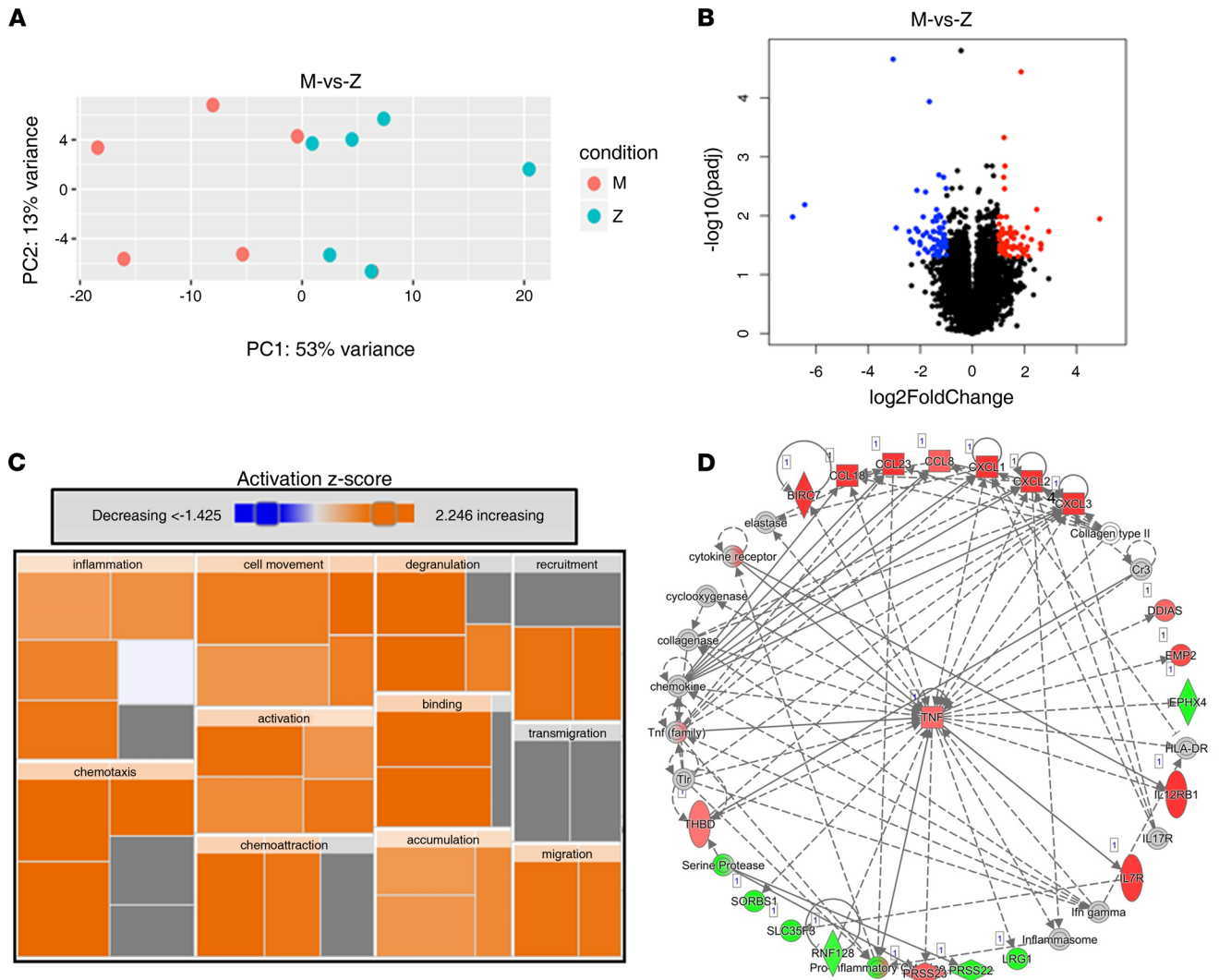


Figure 1. Transcriptome analysis of MDMs. Total RNAs of M- and Z-MDMs were subjected to RNA-Seq, and the data were analyzed using DESeq2. (A) PCA plot depicts relative similarities between M-MDMs samples (red) and Z-MDMs samples (blue). (B) Volcano plot visualizes upregulated (red) or downregulated (blue) genes, which are statistically significant in Z-MDMs. The most statistically significant genes are toward the top. (C) Treemap presents hierarchical heat map of affected downstream functional categories based on DEGs in Z-MDMs. (D) A network of molecules that are related to the biological processes activated in Z-MDMs. Red and green indicate upregulated and downregulated genes in Z-MDMs, respectively.

The expression of NLRP3 is dependent on TLR7 and NF-κB in Z-MDMs. To examine whether the activation of TLR7 is responsible for the increased expression of *NLRP3* in Z-MDMs, we incubated MDMs with oligodeoxynucleotide (ODN) 2088, a TLR7 antagonist, and compared the expression level of *NLRP3* between M- and Z-MDMs. Figure 6A shows that the expression level of *NLRP3* is significantly higher in nonstimulated Z-MDMs than M-MDMs ($P = 0.026$), but the expression level of *NLRP3* is not statistically different between the 2 different MDM groups when the activation of TLR7 was inhibited by ODN 2088 in the cells. The expression level of *NLRP3* was reduced by the ODN 2088 treatment in both M- and Z-MDMs. It indicates that TLR7 positively regulates the expression of *NLRP3* in MDMs, and the activation of TLR7 is responsible for the increased expression of *NLRP3* in Z-MDMs. Since NF-κB is a transcription factor to induce the expression of *NLRP3*, it was intriguing to examine whether TLR7-induced expression of *NLRP3* is dependent on the activation of NF-κB. QNZ is a potent NF-κB inhibitor, and therefore, the activation of NF-κB signaling could be inhibited in QNZ-treated cells. The expression level of *NLRP3* was reduced by QNZ treatment in both M-MDMs and Z-MDMs, and the expression level of *NLRP3* was not statistically different between QNZ-treated M- and Z-MDMs (Figure 6B). The results indicate that NF-κB positively regulates the expression of *NLRP3*, and TLR7-induced expression of *NLRP3* is dependent on the activation of NF-κB.

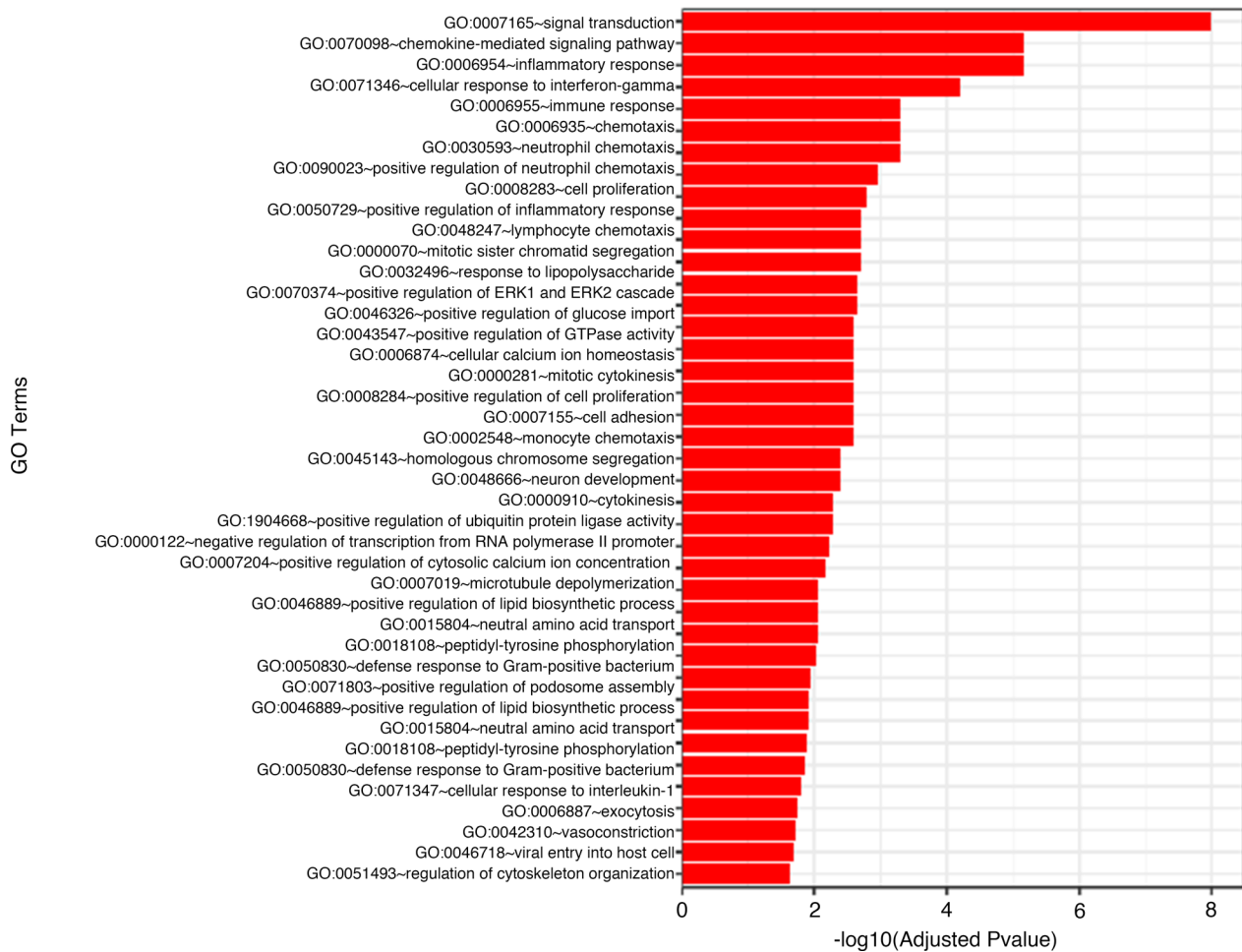


Figure 2. Gene ontology analysis. GO enrichment analysis of DEGs of Z-MDMs compared with M-MDMs was conducted. Significantly differentially expressed genes were clustered by their gene ontology, and top 40 GO terms of Z-MDMs are shown in the figure.

Correlation between the expression levels of Z-AAT and NLRP3. The mutation in the AAT gene substantially reduces AAT secretion from Z-MDMs; thus, Z-AAT accumulates in the cells, causing cytotoxic stress, and increases the expression of proinflammatory cytokines. A previous study about Z-AAT found that Z-AATs indeed accumulate in MDMs. We suspected that Z-AAT could be responsible for the increased expression of NLRPs in Z-MDMs. By analyzing RNA-Seq data of MDMs, we found that the expression level of *NLRP3* was increased as the expression level of AAT was increased in Z-MDMs. The correlation coefficient between the expression levels of the 2 genes was 0.93 in Z-MDMs, but it was 0.49 in M-MDMs. The expression of *NLRP3* was highly correlated with the expression of *TLR7* in both M- and Z-MDMs. To experimentally verify the correlation between the expression levels of Z-AAT and *NLRP3*, we increased the expression level of Z-AAT in Z-MDMs by transfecting the cells with Z-AAT gene-containing plasmid and examined the expression level of *NLRP3* in the transfected cells. The result shows that the expression level of *NLRP3* was increased as the expression level of Z-AAT was increased in the cells. The correlation coefficient between the expression levels of the 2 genes was 0.96, and the *P* value was 0.02, indicating that the expression level of Z-AAT is highly correlated with the expression level of *NLRP3* in Z-MDMs (Figure 7, A and B).

Alu elements upregulated in Z-MDMs. *Alu* is the most abundant transposable element in the human genome, with more than 1 million copies dispersed throughout the human genome (36). There is accumulating evidence that endogenous *Alu* RNA can activate *TLR7* signaling. *TLR7* contains 2 distinct ligand binding sites. One of the binding sites (site 1) binds to guanosine, and the other (site 2) binds to uridine-containing single-stranded RNA (37). The ligand binding sites of *TLR7* are exposed to endosomal lumen. *Alu* RNAs get access to the endosomal *TLR7* through autophagy and bind to the site 2. The binding of *Alu* RNA to the site 2 primes *TLR7* for interaction with guanosine at the site 1 and subsequent dimerization of *TLR7*, leading to *TLR7* activation (23).

Table 1. The upstream regulator analysis in Z-MDMs

Upstream regulator	Activation Z score	P value of overlap	Target molecules in data set
<i>Salmonella enterica</i> serotype abortus equi lipopolysaccharide	2.976	0.000000355	CCL18, CCL23, CXCL1, CXCL2, CXCL3, IL-7R, NLRP3, RHOU, TNF
Peptidoglycan	2.58	0.00000243	CCL18, CCL8, CXCL1, CXCL2, CXCL3, NLRP3, TNF
Vegf	3.07	0.00000377	ACE, BIRC7, CDC20, CXCL1, EMP2, EPHX4, HTR7, IGFBP4, KITLG, MFSD4A
IL-13	2.404	0.0000107	CCL18, CCL23, CD209, COL18A1, CXCL1, CXCL2, CXCL3, HSD11B1, KITLG, MRC1
CSF2	3.246	0.000013	ACE, CCL18, CCL23, CD209, CDC20, CXCL1, CXCL2, MRC1, NLRP3, PLK1
NF-κB (complex)	2.429	0.0000413	CCL8, COL18A1, CXCL1, CXCL2, CXCL3, EDNRB, FUCA1, IL-7R, LIF, PLK1
<i>E. coli</i> LPS	2.229	0.0000478	CCL8, CXCL1, CXCL2, CXCL3, TNF
<i>Salmonella minnesota</i> R595 LPS	2.389	0.0000513	CCL8, CXCL1, CXCL2, CXCL3, EDNRB, TNF
SPP1	2.578	0.0000631	CCL18, CDC20, CXCL1, CXCL2, CXCL3, LIF, TNF
CXCL8	2.236	0.0000788	COL18A1, CR1, CXCL2, CXCL3, TNF
5-O-mycolyl-beta-araf-(1->2)-5-O-mycolyl-α-araf-(1->1′)-glycerol	2.236	0.0000992	CCL8, CXCL1, CXCL2, CXCL3, TNF
Forskolin	2.397	0.000131	ACE, ACPP, ARHGEF5, BIRC7, CCL18, COL18A1, CXCL1, CXCL2, CXCL3, HSD11B1
Cardiotoxin	2	0.000174	EDNRB, IL-7R, MRC1, PIGR, TNF, TNNT1
Tetradecanoylphorbol acetate	3.18	0.000205	ACE, CCL18, CD209, CE51, CXCL2, CXCL3, GSTM1, HSD11B1, HTR7, IL-12RB1
HGF	2.559	0.000394	CDC20, CXCL2, EMP2, HTR7, IGFBP4, KITLG, PLK1, SLC1A2, THBD, TNF
EGR1	2.176	0.000548	ACE, CDC20, CXCL2, CXCL3, ME1, TNF
Poly rI:rC-RNA	2.035	0.000647	CCL8, CD209, CXCL1, CXCL2, CXCL3, LIF, NLRP3, PIGR, SFXN2, TNF
MYD88	2.085	0.000664	ACPP, CXCL1, CXCL2, CXCL3, EDNRB, MRC1, TNF
FN1	2.406	0.000931	ACE, CD79A, CXCL1, CXCL2, CXCL3, TNF
TLR7	2.184	0.00119	CD79A, CREB5, CXCL1, CXCL2, CXCL3, TNF
cytokine	2	0.00148	ANG, CD209, CXCL1, CXCL3, LIF
APP	2.045	0.00399	AP3B2, COL18A1, CXCL1, CXCL2, CXCL3, GPR85, LIF, MRC1, PLK1, SLC1A2
FAS	2.191	0.0164	COL18A1, CXCL1, CXCL2, CXCL3, THBD, TNF
<i>E. coli</i> B4 LPS	2.153	0.019	CXCL2, CXCL3, DDIAS, MRC1, TNF
CEBPB	2.103	0.0801	CXCL2, CXCL3, HSD11B1, IGFBP4, TNF

It was experimentally verified that overexpressed *Alu* elements activate endosomal TLR7, and the activated TLR7 induces the expression of proinflammatory cytokines including TNF- α (22). RNA-Seq analysis of MDMs found in this study that the expression level of *TNFA* is significantly higher in Z-MDMs than M-MDMs. It was previously found that *Alu* RNAs induce the expression of proinflammatory cytokines through TLR7 activation in patients with systemic lupus erythematosus. The study also found that *Alu* RNAs are upregulated in autoimmune diseases (22). Since cellular stresses induce the transcription of *Alu* elements and Z-AAT causes ER stress (8, 38), we suspected that the transcription rate of the *Alu* element is higher in Z-MDMs than M-MDMs. We compared the normalized read count of *Alu* transcript between M- and Z-MDMs and found that the transcription rate of *Alu* elements was significantly higher in Z-MDMs than M-MDMs (Figure 8A; $P = 0.0152$). One of the previous studies about TLR7 found that the UUC motif and UUG motif have full binding affinity and moderate binding affinity to TLR7, respectively (39). We scrutinized the nucleotide sequences of *Alu* elements to examine whether the elements have the TLR7 binding motifs. *Alu* elements are largely divided into 3 different subfamilies: *AluJ*, *AluS*, and *AluY* (40). As shown in Supplemental Figure 2, *AluJ* and *AluS* subfamilies contain both UUC and UUG motifs, while *AluY* contains only the UUG motif. We also compared the normalized read number of each *Alu* subfamily between M- and Z-MDMs. The result shows that reads per million mapped reads (RPM) of *AluJ* is significantly higher in Z-MDMs than M-MDMs (Figure 8B; $P = 0.0087$). RPM of *AluS* was, on average, higher in Z-MDM, but there was no statistical difference between the 2 MDM groups ($P = 0.0931$).

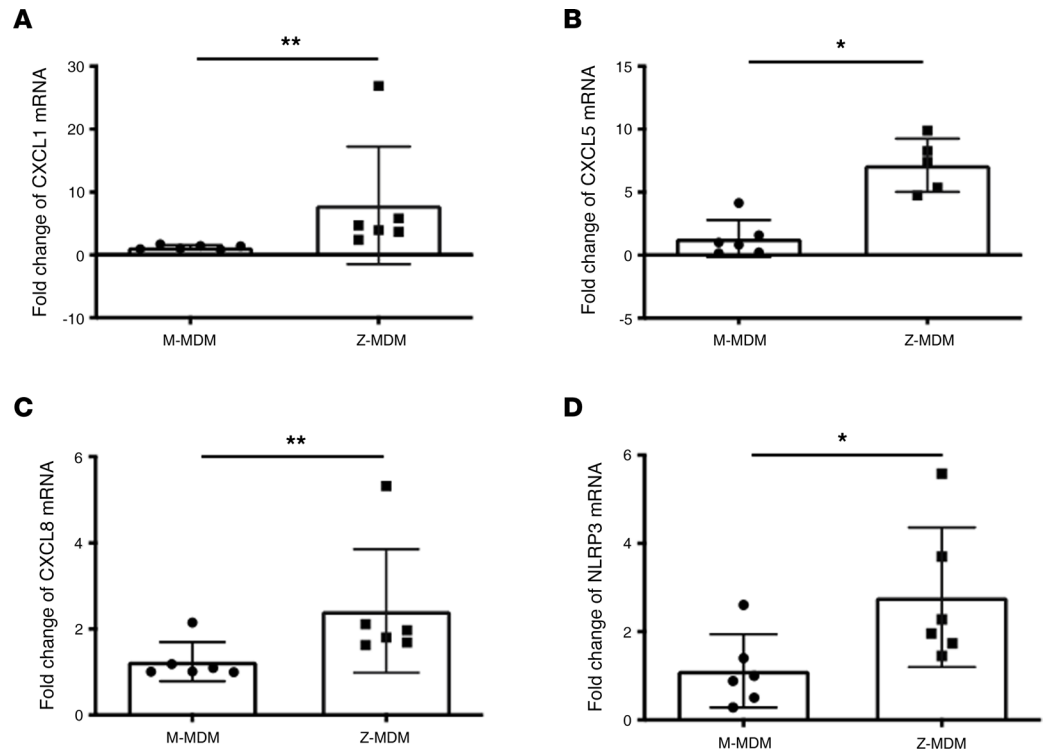


Figure 3. Verification of the DEGs by qPCR. DEGs identified using RNA-Seq were validated using qPCR. (A–C) Relative expression of neutrophil chemoattractant factors in Z-MDMs ($n = 6$, circles) versus M-MDMs ($n = 6$, squares) is represented by fold change. (D) Relative expression of NLRP3 in Z-MDMs ($n = 6$, circles) versus M-MDMs ($n = 6$, squares) is represented by fold change. Statistical analysis was conducted using the Mann-Whitney U test. Statistical significance is denoted by $*P < 0.05$ and $**P < 0.01$.

RPM of *AluY* was similar between them. We analyzed the top 500 *Alu* elements to identify *Alu* elements that are upregulated in Z-MDMs. The result found that the transcripts of 29 *Alu* loci are abundant in both MDM groups but significantly upregulated in Z-MDMs. We analyzed the subfamily and genomic location of the 29 *Alu* elements and found that the *Alu* elements are randomly distributed over different chromosomes, but most of them belong to either *AluJ* or *AluS* subfamily (Figure 8C). The chromosomal distribution of the *Alu* elements is visualized in Supplemental Figure 3. In order for *Alu* RNA to activate TLR7, they need to be internalized in endosomes. We isolated endosomes from M- and Z-MDMs to compare the level of endosomal *Alu* RNA between the 2 MDM groups. The result shows that the level of endosomal *Alu* RNA is significantly higher in Z-MDMs than M-MDMs (Figure 8D; $P = 0.0022$). It indicates that there is an increased *Alu* RNA to activate endosomal TLR7 signaling in Z-MDMs.

Accelerated death of ZZ monocytes. *Alu* RNAs of apoptotic cells could be transported to the phagosome of macrophages when the macrophages phagocytose the apoptotic cells, and the *Alu* RNAs could activate TLR7 signaling in the phagocytosing macrophages. During in vitro macrophage differentiation, MDMs phagocytose dead monocytes, and *Alu* RNAs of the dead monocytes could be transported to the endosome of the MDMs, leading to the activation of endosomal TLR7 in MDMs. When monocytes were incubated in macrophage differentiation media, some of monocytes are successfully differentiated into macrophages, but others go to either apoptosis or necrosis. The dead monocytes will be phagocytosed by MDMs so that *Alu* RNAs of dead monocytes get access to endosomal TLRs in MDMs. As the number of dead monocytes is increased, the probability for *Alu* RNAs to activate TLR7 signaling in macrophages is increased during MDM differentiation. It was previously found that the apoptosis rate of ZZ neutrophils is 2-fold higher than MM neutrophils because Z-AAT induces cell death by inducing the expression of TNF- α and by increasing ADAM-17 activity (15). To explain the higher level of endosomal *Alu* RNA in Z-MDMs, we measured and compared the percentage of dead monocytes between M-MDM and Z-MDM cultures. Using flow cytometry, the percentage of dead monocytes was measured immediately after we isolated monocytes using a monocyte enrichment kit. Figure 9, A and B, show a

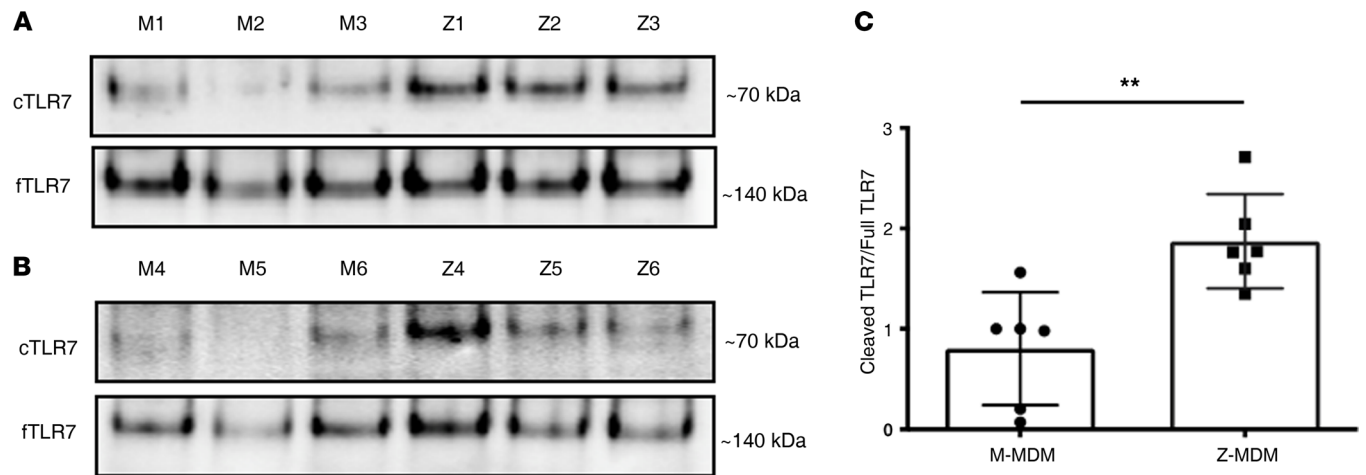


Figure 4. The activation of TLR7 in Z-MDMs. MDMs were collected at day 7 of macrophage differentiation, and total proteins were isolated from the collected cells. **(A and B)** Equal amounts of total proteins of M- and Z-MDMs were analyzed via native-PAGE of cleaved and full-length TLR7, and protein band intensities of cleaved and full-length TLR7 were compared in M- and Z-MDMs ($n = 6$). **(C)** The protein band intensities were measured using NIH ImageJ software and presented as a ratio of cleaved to full-length TLR7. Statistical analysis was conducted using the Mann-Whitney U test. Statistical significance is denoted by $**P < 0.01$.

representative flow cytometry image of a MM monocyte and ZZ monocyte, respectively. The death rate of ZZ monocytes was significantly higher than that of MM monocytes on day 0 (Figure 9C; $P = 0.026$). We incubated the isolated monocytes in macrophage differentiation media for 24 hours and measured the rate of dead cells in M-MDM and Z-MDM cultures (day 1). Compared with the cell death rate on day 0, the death rate was increased on day 1 in both M-MDM and Z-MDM cultures (Figure 9, D and E). The increased rates were 1.3% and 4.7% in M-MDM and Z-MDM cultures, respectively. The percentage of dead cells was significantly higher in Z-MDM culture than M-MDM culture on day 1 (Figure 9F; $P = 0.0411$). Overall, the result shows that the cell death rate of monocytes is significantly higher in Z-MDM than in M-MDM culture. The higher level of dead monocytes in Z-MDM culture would, in part, explain the higher level of endosomal *Alu* RNA in Z-MDMs.

Discussion

The Glu to Lys substitution at residue 342 in the AAT protein leads to a low concentration of AAT in circulating blood so that AAT does not reach lung tissues where it functions as the primary defense against proteolytic activities of a serine protease in AATD individuals. A serum AAT level of 11 μM represents the protective threshold value below which the risk of lung diseases is believed to increase. The concentration of circulating AAT is 20–53 μM in normal individuals but ranges from 3 μM to 7 μM in AATD individuals with homozygous Z mutant allele, leading to progressive lung parenchyma destruction and rapid decline in lung function over time (14, 41). The number of alveolar neutrophils is increased in the lung of AATD individuals. The increased number of alveolar neutrophils subsequently increases the concentration of neutrophil elastases, resulting in the imbalance between proteases and antiprotease in the lower respiratory tract of AATD individuals (42). Therefore, previous studies have focused on the imbalance between proteases and antiprotease to elucidate the pathogenesis of lung diseases associated with AATD while the toxic gain-of-function of intracellular Z-AAT has been overlooked in developing lung diseases. However, it was recently found that the expression levels of inflammatory cytokines such as TNF- α , CXCL1, and CXCL8 are significantly higher in Z-MDMs than M-MDMs (18). CXCL1 and CXCL8 are neutrophil chemoattractant factors; thus, the higher expression levels of the chemokines are able to attract more neutrophils into the pulmonary alveoli of AATD individuals, enhancing neutrophil-related inflammation. TNF- α is known to induce cell death (43). The higher expression levels of those cytokines in Z-MDMs indicate that the imbalance between proteases and antiprotease is not the only cause to induce proinflammatory signaling in the lung of AATD individuals. Although AAT is known to have an antiinflammatory function, it was experimentally demonstrated that extracellularly added AAT was not able to reduce the expression of the inflammatory chemokines, and this also supports that a low concentration of extracellular AAT is

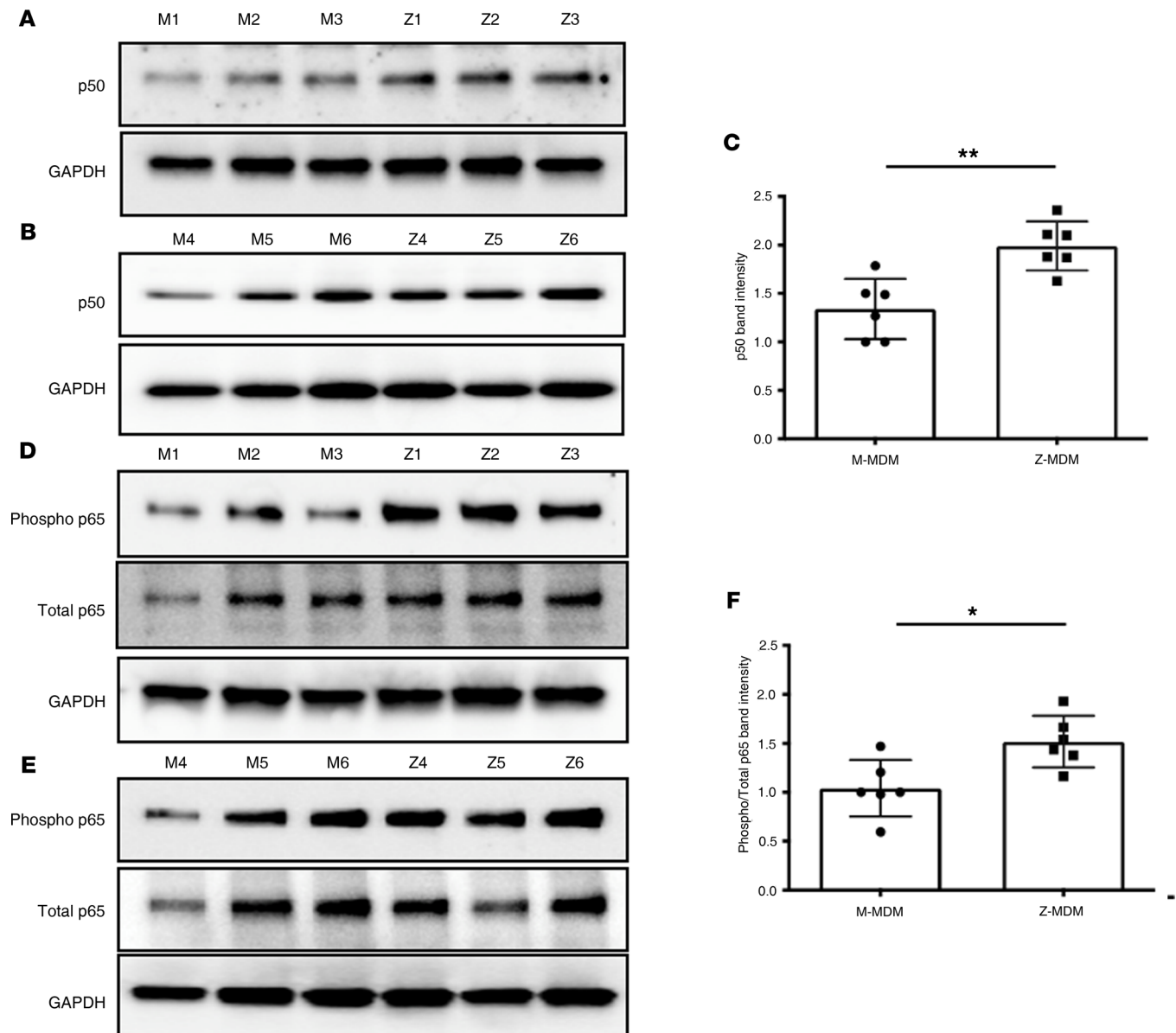


Figure 5. NF- κ B signaling activated in Z-MDMs. Total proteins were isolated from MDMs and subjected to SDS-PAGE to examine the activation of NF- κ B signaling in Z-MDMs. (A-C) p50 is an indicator for the activation of NF- κ B signaling so the level of p50 was analyzed via SDS-PAGE (A and B) and compared using NIH ImageJ software (C). (D and E) The phosphorylated form of p65, another indicator for NF- κ B activation, was also analyzed using western blotting. The protein band intensities of phosphorylated p65 and total p65 were quantified using NIH ImageJ software. (F) To examine the activation of NF- κ B signaling, a ratio of phosphorylated p65 to total p65 was matured in MDM samples and compared between M-MDMs and Z-MDMs. Statistical analysis was conducted using the Mann-Whitney *U* test. Statistical significance is denoted by **P* < 0.05 and ***P* < 0.01.

not responsible for the increased expression of the inflammatory cytokines in Z-MDMs. When MDMs were incubated with LPS, the LPS treatment enhanced inflammatory signaling in both M- and Z-MDMs, but the increased expression levels of inflammatory cytokines were significantly higher in Z-MDMs than M-MDMs (18). Those findings also support that a low concentration of AAT, which are uncontrolled proteolytic activities of neutrophil proteases, is not a sole cause for the higher concentration of proinflammatory cytokines observed in the lower respiratory tract of AATD individuals. Therefore, we propose that the toxic gain of function of intracellular Z-AAT contributes to the higher expression levels of inflammatory cytokines and primes alveolar macrophages for proinflammatory signaling.

In this study, we conducted RNA-Seq of M- and Z-MDMs. By analyzing the RNA-Seq data, we hypothesized that TLR7 and NF- κ B signaling are activated in Z-MDMs, and we experimentally verified that

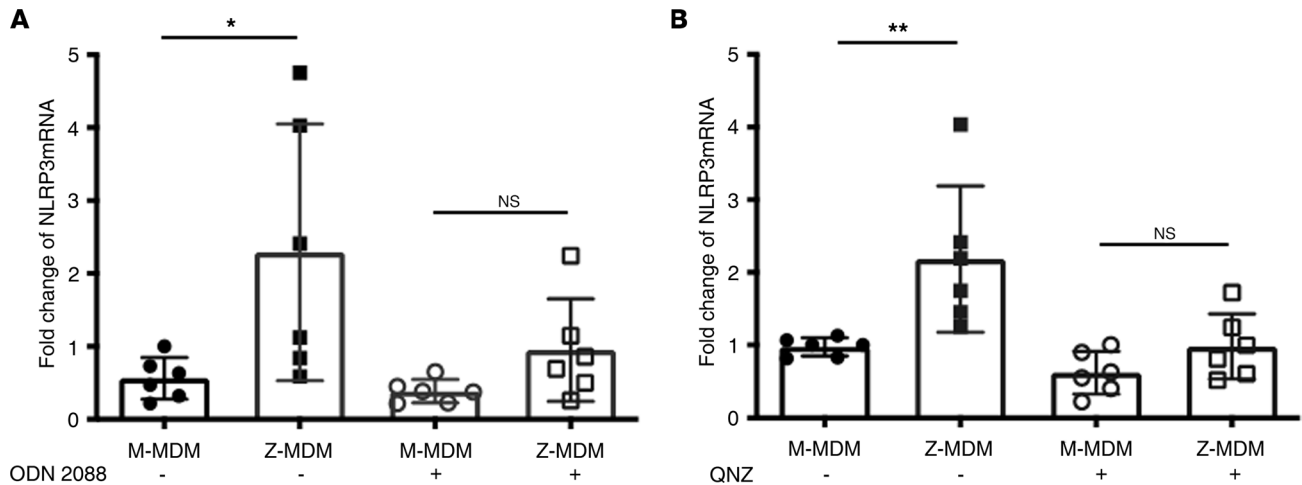


Figure 6. The expression of NLRP3 dependent on TLR7 and NF- κ B signaling. (A) MDMs were differentiated for 7 days and incubated with 1 μ M of ODN 2088 overnight. MDM controls were incubated with 1 μ M of ODN 2088 control overnight. Using qPCR, the expression levels of *NLRP3* were compared between untreated M- and Z-MDMs. ODN 2088 inhibits the activation of TLR7 signaling. When the activation of TLR7 was inhibited by ODN 2088, the expression levels of *NLRP3* were also compared between the 2 MDM groups. (B) MDMs were incubated with 25 nM of QNZ overnight. QNZ inhibits the activation of NLRP3 signaling. The expression levels of *NLRP3* were compared between M- and Z-MDMs before and after QNZ treatment. Statistical analysis was conducted using the Mann-Whitney *U* test. Statistical significance is denoted by * $P < 0.05$ and ** $P < 0.01$.

the inflammatory signaling is activated and subsequently induces the expression of NLRP3 in Z-MDMs. Indeed, it is not a new concept that Z-AAT is associated with the activation of NF- κ B signaling. One of the previous studies on Z-AAT transfected CHO cells with Z-AAT plasmid and found that the overexpression of Z-AAT activates NF- κ B signaling in the transfected cells (44). In addition, another study found that NF- κ B signaling is activated in mice that were genetically modified to have a human Z-AAT gene (45), indicating that the activation of NF- κ B signaling by Z-AAT is not limited to in vitro cell culture but is also seen in vivo. NLRP3 is an intracellular sensor to detect a broad range of microbial motifs and endogenous danger signals, leading to the formation and activation of the NLRP3 inflammasome. NLRP3 inflammasome is a well-studied inflammasome and has been associated with various diseases characterized by chronic inflammation, such as autoinflammatory diseases and atherosclerosis (46). To date, a 2-signal model has been proposed for NLRP3 inflammasome activation. A first signal, which could emanate from microbial components or endogenous ligands, primes the activation of NF- κ B signaling and subsequent upregulation of NLRP3 and pro-IL-1 β . A second signal from extracellular ATP or toxins activates the NLRP3 inflammasome (47). In this study, we found that the expression level of *NLRP3* is significantly higher in Z-MDMs than in M-MDMs, while the expression level of *IL-1* is not statistically different between the 2 MDM groups. Interestingly, a similar expression pattern of NLRP3 and IL-1 was reported in a previous study on stable chronic obstructive pulmonary disease (COPD). The expression level of NLRP3 was significantly higher in the lungs of stable patients with COPD than controls, but the expression level of IL-1 β was statistically similar between the 2 groups (48). The Z-AAT allele is most commonly associated with severe AATD, and AATD is a predisposing factor to the development of COPD. Hence, it is very intriguing that Z-MDM and alveolar macrophages of patients with COPD show a similar profiling in the expression of the inflammatory molecules. It is known that individuals who are homozygous for the Z-AAT allele have an increased chance of developing COPD. Because a secondary stimulator such as bacterial infection induces the expression of IL-1 β and activates NLRP3 inflammasome, the higher expression level of *NLRP3* in Z-MDMs might explain for chronic inflammation in the lungs of individuals homozygous for the Z-AAT allele.

It was previously suggested that NF- κ B signaling is activated, and the activated NF- κ B induces the expression of NLRP3 in the lung of AATD individuals (49). However, the mechanism that is responsible for the increased level of NLRP3 has not been studied. In the present study, we found that TLR7 signaling is activated in Z-MDMs, and the activated TLR7 signaling induces the expression of NLRP3 in the cells. We suspect that *Alu* elements activate TLR7, and the activated TLR7 subsequently activates NF- κ B to induce the expression of NLRP3 in Z-MDMs. The ligand binding site of TLR7 locates toward the endosomal lumen preventing endogenous RNAs from binding to endosomal TLR7. However, it was

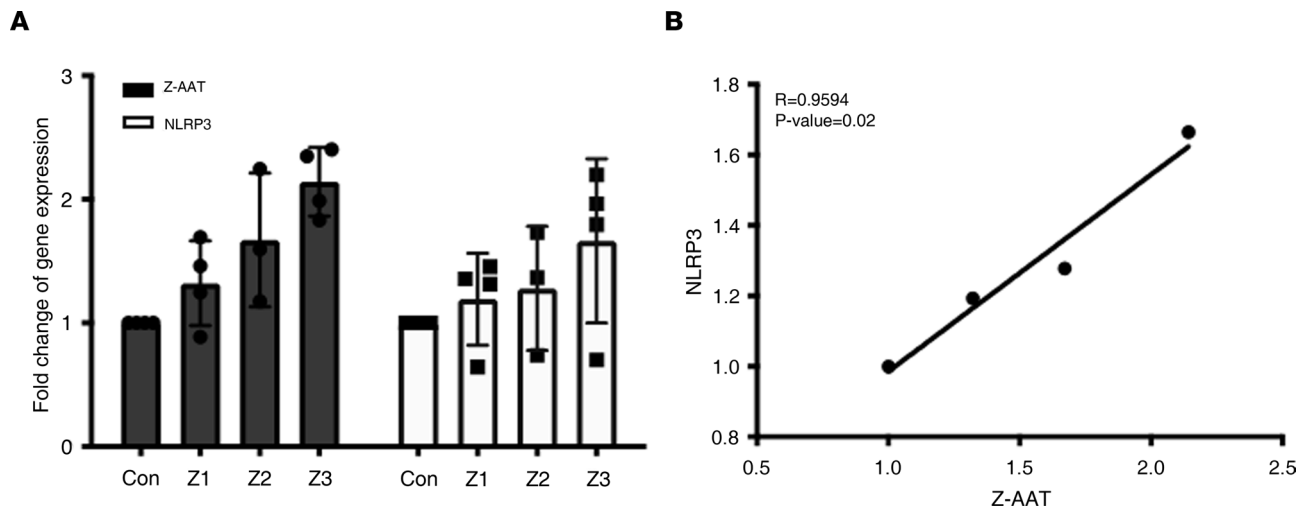


Figure 7. Positive correlation between the expression levels of Z-AAT and NLRP3 in Z-MDMs. Z-MDMs were transfected with 3 different concentrations of Z-AAT gene-containing PCR3.1 plasmids: Z1, 350 ng; Z2, 550 ng; and Z3, 750 ng. The MDM control was transfected with the PCR3.1 plasmid without the Z-AAT gene. Total RNAs were isolated from the transfected cells at 48 hours after transfection. (A) Using qPCR, the relative expression levels of AAT and NLRP3 were examined in untransfected controls and cells transfected with the Z-AAT gene-containing plasmid. (B) A Pearson's correlation coefficient and P value between the expression levels of NLRP3 and AAT were calculated in Z-MDMs using GraphPad Prism.

experimentally proven that *Alu* RNAs are able to get an access to endosomal TLR7 through autophagy. The human genome contains more than 1 million copies of *Alu* elements, and they represent approximately 10% of the human genomic DNA. Therefore, the majority of transcribed human pre-mRNAs contain a surprisingly high number of *Alu* elements. The present study found that the level of endosomal *Alu* RNA is significantly higher in Z-MDMs than in M-MDMs. We propose 2 different mechanisms to explain the higher level of endosomal *Alu* RNA in Z-MDMs, shown in Figure 10. First, the transcription rate of the *Alu* element is higher in Z-MDMs than M-MDMs. The transcription rate of the *Alu* element is increased in response to various factors such as cellular stresses and viral infections. We suspect that cellular stress caused by Z-AAT increases the transcription rate of the *Alu* element. It was previously reported that Z-AAT accumulates in the ER of monocytes, leading to ER stress (16). Second, the probability for *Alu* RNAs of apoptotic cells to go to the endosome of phagocytes is higher with Z-MDMs than M-MDMs. It was previously determined that *Alu* RNAs of apoptotic cells could travel to endosomes of macrophages, while the macrophage phagocytoses the apoptotic cell (50). Considering that the cell death rate of ZZ monocytes is higher than that of MM monocytes, and the efferocytosis ability is similar between unstimulated M- and Z-MDMs (18), Z-MDMs phagocytose more apoptotic cells and, therefore, have more *Alu* RNAs of apoptotic cells to travel to the endosome of Z-MDMs. AAT is known to inhibit autophagy (51), while the accumulation of Z-AAT promotes autophagy (52). Z-AAT-induced autophagy will promote the delivery of *Alu* RNA to endosomes, which subsequently increases the chance of *Alu* RNA as an endogenous ligand to activate endosomal TLR7 signaling. Thus, we could not rule out that autophagy is activated in Z-MDMs, delivering more *Alu* RNAs to the endosome.

AAT mutations have been associated with chronic airway inflammation. It was traditionally believed that loss or reduction in AAT concentration resulting from the mutations make AATD individuals more susceptible to chronic airway inflammation because AAT is a serine protease inhibitor and has antiinflammatory functions (53). However, findings from this study highlight the possibility that the toxic gain of function of Z-AAT could be a significant driver of inflammation in the lower respiratory tract of AATD individuals. This study demonstrates that Z-AAT activates, directly or indirectly, TLR7 signaling, and the activated TLR7 induces the expression of NLRP3, which could predispose AATD individuals to lower respiratory tract inflammation. We have determined TLR7 signaling as a potentially novel mechanism that is responsible for the toxic gain of function of Z-AAT in alveolar macrophages. Aberrant activation of TLR7 is a potential pathogenic factor and has been linked to certain human diseases. Thus, modulation of TLR7 signaling would inhibit chronic inflammation in the lower respiratory tract of AATD individuals with a homozygous Z mutant allele. The findings of this study will contribute to elucidating more details in the pathogenesis of Z-AAT-associated

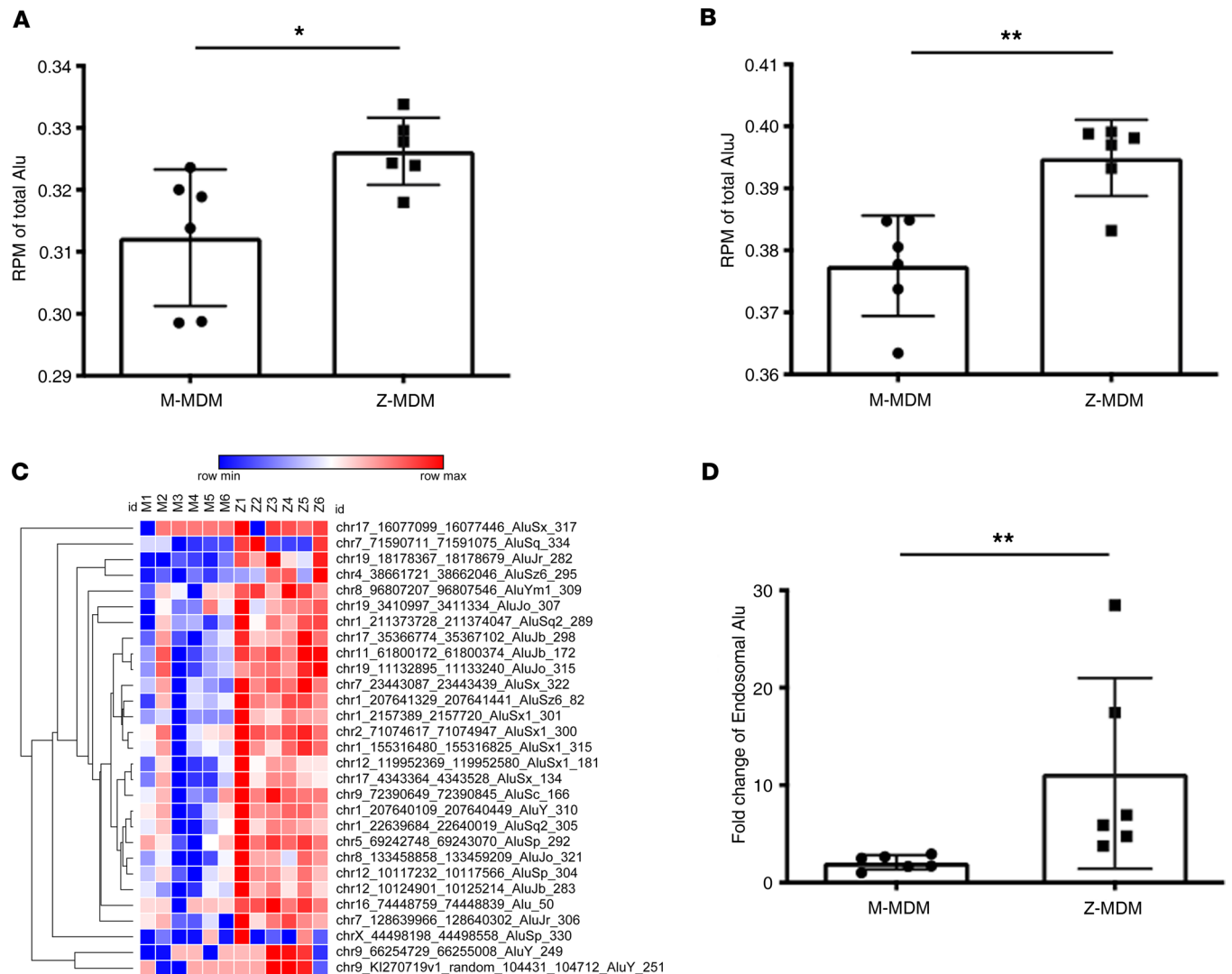


Figure 8. Increased transcription rate of *Alu* elements in Z-MDMs. (A) The transcription rates of *Alu* elements were normalized using RPM, and RPM of *Alu* elements was compared between M- and Z-MDMs. (B) RPM of *AluJ*, one of *Alu* subfamilies, was compared between M- and Z-MDMs. (C) *Alu* elements much more abundant in Z-MDMs than M-MDMs were identified, and their genomic locations were examined. (D) Endosomes were isolated from MDMs, and RNAs were retrieved from the isolated endosomes. Using qPCR, the level of endosomal *Alu* RNAs was compared between M- and Z-MDMs. Statistical analysis was conducted using the Mann-Whitney *U* test. Statistical significance is denoted by * $P < 0.05$ and ** $P < 0.01$.

lung diseases. Therefore, the knowledge gained from this study may have significant implications for future therapeutic strategies for chronic airway inflammation in AATD individuals.

Methods

Monocyte isolation and macrophage differentiation. Blood samples were collected from outpatient volunteers (University of Florida) using Sodium citrate tubes, and PBMCs were isolated from the blood using Ficoll-gradient centrifugation (400g at 18°C for 30 minutes). Characteristics of the volunteers are shown in Table 2. None of them were under AAT augmentation therapy. Monocytes were purified from the PBMCs using a monocyte enrichment kit (Stemcell Technologies), following the manufacturer's instructions. Monocytes were plated in 12-well plates at 300,000 cells per well in macrophage differentiation media (RPMI 1640 containing 10% FBS, 100 units/mL penicillin, 100 µg/mL streptomycin, 250 ng/mL amphotericin B, recombinant human GM-CSF [0.5 ng/mL], and recombinant human M-CSF [5 ng/mL][all from Gibco]) and differentiated for 7 days. Supplemental medium (50% of the volume in each well) was added every 3 days after removing half of the old media, and cells were used on day 7 for any treatment. MDMs were harvested for RNA extraction using the Qiagen RNeasy kit (Qiagen).

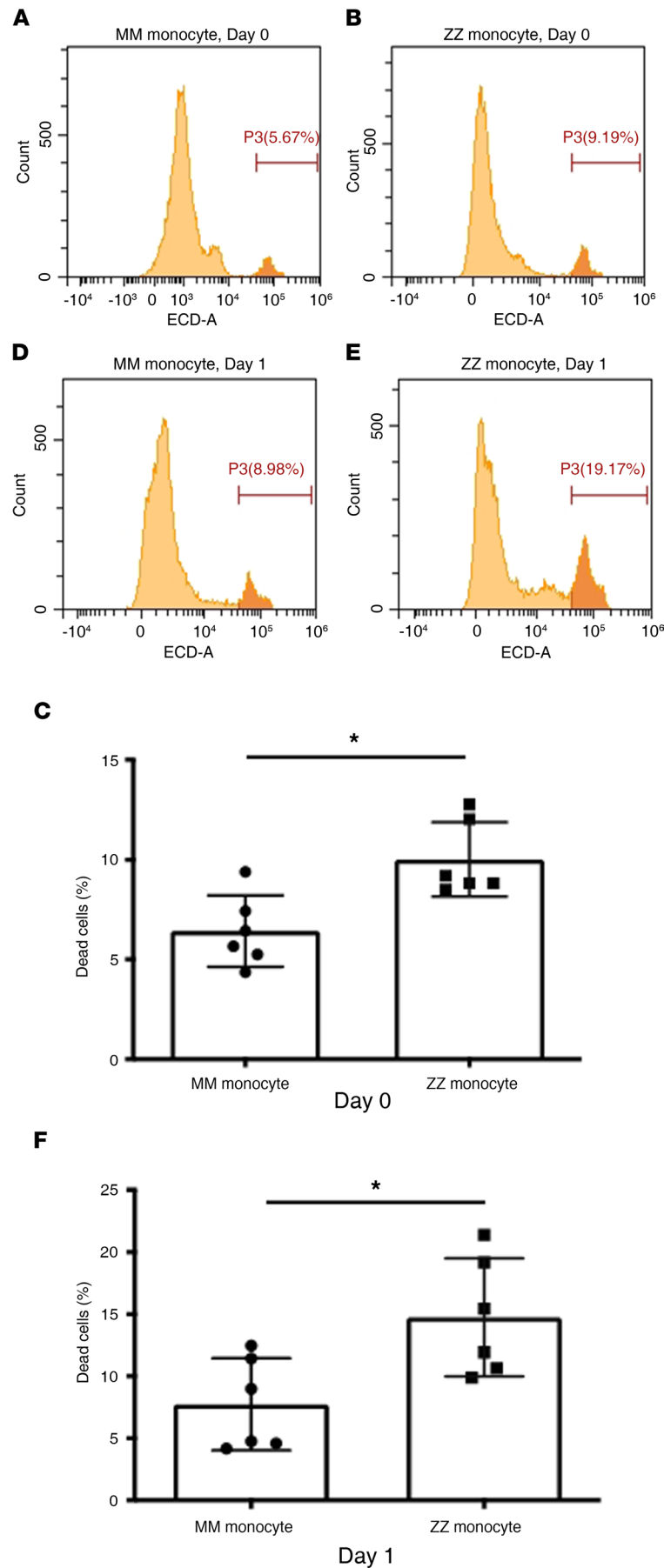


Figure 9. Accelerated death rate of monocytes homozygous for Z-AAT allele. Monocytes were isolated from PBMC, and the percentage of dead monocytes was assessed by flow cytometric analysis. (A-C) For day 0, MM monocytes (A) and ZZ monocytes (B) were labeled with EthD-1 immediately after their isolation from PBMC, and the percentage of dead cells were compared between the 2 monocyte groups (C). (D and E) For day 1, MM monocytes (D) and ZZ monocytes (E) were incubated in macrophage differentiation media for 24 hours and labeled with EthD-1. (F) The percentage of dead cells was analyzed and compared between MM and ZZ monocytes. Statistical analysis was conducted using the Mann-Whitney *U* test. Statistical significance is denoted by **P* < 0.05.

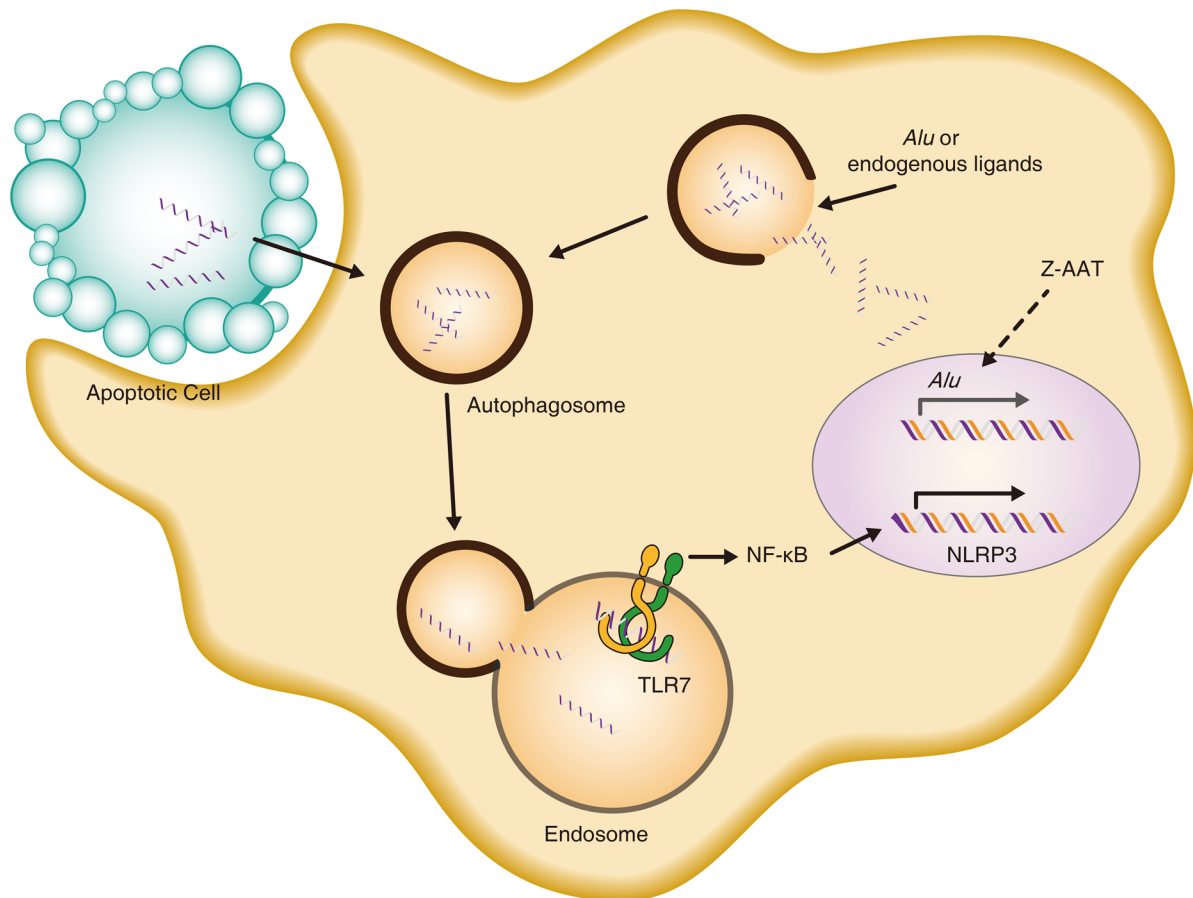


Figure 10. Proposed model of *Alu* element as an endogenous ligand for TLR7 activation in Z-MDMs.

RNA-Seq and data analysis. Total RNAs of 6 different M-MDMs and 6 different Z-MDMs were subjected to RNA-Seq. RNA integrity was examined using Agilent TapeStation 4200 (Agilent Technologies,). RNA-Seq libraries were prepared using the NEBNext Ultra RNA Library Prep Kit for Illumina following the manufacturer's instructions (NEB). The sequencing libraries were clustered on 2 lanes of a flowcell. After clustering, the flowcell was loaded on the Illumina HiSeq instrument (4000 or equivalent) according to manufacturer's instructions. The samples were sequenced using a 2×150 bp paired-end (PE) configuration. Image analysis and base calling were conducted by the HiSeq Control Software (HCS). The sequence read was trimmed to remove possible adapter sequences and nucleotides with poor quality using Trimmomatic v.0.36. The trimmed reads were mapped to the *Homo sapiens* reference genome available on ENSEMBL using the STAR aligner v.2.5.2b. Unique gene hit counts were calculated by using feature Counts from the Subread package v.1.5.2. Only unique reads that fall within exon regions were counted. After extraction of gene hit counts, the gene hit counts table was used for downstream differential expression analysis. Using DESeq2, a comparison of gene expression between the groups of samples was performed. The Wald test was used to generate *P* values and \log_2 fold changes. Genes with adjusted *P* < 0.05 and absolute \log_2 fold changes > 1 were called as DEGs for each comparison. A GO analysis was performed on the statistically significant set of genes by implementing the software GeneSCF. The goa_human GO list was used to cluster the set of genes based on their biological process and determine their statistical significance. A PCA was performed using the "plotPCA" function within the DESeq2 R package. The plot shows the samples in a 2D plane spanned by their first 2 principal components. The top 500 genes, selected by highest row variance, were used to generate the plot. RNA-Seq of MDMs were conducted and analyzed by Genewiz. RNA-Seq data are deposited at NCBI under the bioproject accession number PRJNA788574.

Western blot analysis. Total proteins were extracted from MDMs using RIPA lysis buffer (Cell Signaling Technology) with 0.1% SDS, protease, and phosphatase inhibitors. The protein concentration of each sample was measured using a standard Bradford assay (Bio-Rad) and equal amounts of protein samples were loaded

Table 2. Characteristics of controls and AATD individuals

Characteristic	PiMM (n = 6)	PiZZ (n = 6)	P value
Age	38.5(21–69)	51(35–57)	0.82
Sex (M/F)	3/3	2/4	N/A
FEV ₁ % predicted	102.4 (97–111)	81.1 (47.9–102)	0.074
FEV ₁ /FVC	83.3 (74–91)	56.6 (40–75)	0.0043
Current smoker	No	No	N/A

PiMM, individuals homozygous for normal PiM allele; PiZZ, individuals homozygous for mutant PiZ allele; FEV₁, forced expiratory volume in 1 second; FVC, forced vital capacity.

onto a 12% SDS polyacrylamide gel (Bio-Rad). After gel electrophoresis, the proteins were transferred onto a 0.45 µm nitrocellulose membrane using the wet-transfer system, and the membrane was blocked in Tris-buffered saline with 0.1% Tween 20 (TBST) containing 5% nonfat dry milk or 5% BSA for phosphorylated protein. The membrane was immunoblotted overnight at 4°C with primary antibodies (Cell Signaling Technology), p65 (catalog 8242S), phosphor-p65 (catalog 3033S), and p50 (catalog 12540S) at a dilution of 1:1000 in TBST. Horseradish peroxidase conjugated anti-rabbit antibody (catalog 1706515, Bio-Rad) was used for secondary labeling at 1:1,000 in TBST for 1 hour at room temperature. The membrane was probed with GAPDH rabbit polyclonal antibody (catalog 10494-1-AP, Proteintech) at 1: 5000 in TBST. Horseradish peroxidase-conjugated anti-rabbit (catalog 1706515, Bio-Rad) was used for secondary labeling at 1:5000 in TBST for 1 hour at room temperature. Protein bands were visualized by enhanced chemiluminescence (ECL, GE Healthcare). For native gel electrophoresis, total proteins were extracted from MDMs using cell lysis buffer (Cell Signaling Technology) with protease and phosphatase inhibitors. Equal amounts of protein samples were loaded onto a native gel (Invitrogen). After gel electrophoresis, the proteins were transferred onto a 0.45 µm nitrocellulose membrane and immunoblotted with TLR7 antibody (Novus Biologicals) at a dilution of 1:500 in TBST.

Gene expression validation by qPCR. Total RNA (1 µg) extracted from MDMs was reverse transcribed using SuperScript VILO Master Mix (Invitrogen), according to the manufacturer's instruction. Quantification of PCR products was performed with 7500 Fast Real-time PCR (Applied Biosystems). SensiFAST Real-Time PCR Kit (Bioline) was used to produce fluorescence-labeled PCR products and to monitor increasing fluorescence during repetitive cycling of the amplification reaction. Taqman probes/primers specific for the *NLRP3*, *CXCL1*, *CXCL5*, *CXCL8*, and *SERPINA1* genes, and for the *18S rRNA* gene, as internal control, were used in the real-time PCR reaction. Expression levels of the genes were obtained using the classical $2^{-\Delta\Delta Ct}$ method. To compare endosomal *Alu* RNAs between M- and Z-MDMs, primers for *Alu* element were obtained from a previously published research article (22).

Alu expression profiling. Raw quality portions of sequenced reads (by the PE method) were trimmed using Trim galore (version 0.6.6), and trimmed reads were then mapped to all known repeat elements (± 15 bp; annotated by RepeatMasker [<http://www.repeatmasker.org>] using BWA-MEM, version 0.7.17) with default parameters (54). The number of mapped reads on repeat elements were counted using featureCounts (version 2.0.0) with the following parameters: -p -M -O -fraction (55). Expression levels of all *Alu* elements were normalized utilizing the RPM method. Upregulated *Alu* elements were identified using DESeq2 (version 1.30.1) with an adjusted *P* value cutoff of 0.05. Morpheus (<https://software.broadinstitute.org/morpheus/>) was used to cluster upregulated *Alu* elements using the hierarchical clustering method with the one minus Pearson correlation metric. The chromosomal distribution of upregulated *Alu* element in Z-MDMs was visualized using the Idiographica web tool. To visualize potential TLR7 binding motifs on *Alu* elements, 1 member from each *Alu* subfamily was randomly selected, and their consensus sequences were aligned using BioEdit software version 7.2.5.

Endosomal RNA isolation. Ten million monocytes were plated in a 10 cm cell culture dish and differentiated in macrophage differentiation media for 7 days. MDMs were washed with PBS and incubated with Accutase (Stemcell Technologies) at room temperature for 20 minutes. Then, the MDMs were incubated for 15 minutes on ice and collected by gentle scraping with a plastic scraper. The collected cells were washed with cold PBS, and the endosomes were isolated from the MDMs using Minute Endosome Isolation kit, following the manufacturer's instruction (Invent Biotechnologies). The isolated endosomes were lysed using RLT lysis buffer, and endosomal RNAs were isolated from the lysate using RNeasy mini kit with MinElute column (Qiagen).

Transfection. Monocytes were plated in 12-well plates at 300,000 cells per well and differentiated in macrophage differentiation media for 7 days. The differentiated MDMs were transfected with PCR3.1 plasmid with or without Z-AAT gene using PolyJet In Vitro DNA Transfection reagent (SignaGen). Three different concentrations of plasmid, 350 ng, 550 ng, and 750 ng, were used for the transfection, and the plasmids were incubated with PolyJet reagent for 12 minutes. The media of the transfected MDMs were changed 4 hours after the transfection to minimize the cytotoxic effect of the transfection reagent. The transfected MDMs were collected at 48 hours after transfection, and the expression levels of NLRP3 were compared between the MDMs transfected with empty plasmid and with Z-AAT gene-containing plasmid using qPCR.

Percentage of dead monocytes measured by flow cytometry. Monocytes were isolated from individuals homozygous for normal PiM allele (PiMM) and individuals homozygous for mutant PiZ allele (PiZZ) and incubated with 4 μ M of red-fluorescent ethidium homodimer-1 (EthD-1) at room temperature for 15 minutes (day 0). EthD-1 is cell membrane impermeable and is a high-affinity nucleic acid stain. When EthD-1 enters cells with damaged membranes, it undergoes a 40-fold enhancement of fluorescence by binding to nucleic acids, producing a red fluorescence in dead cells. After the incubation, unbound EthD-1 was removed by centrifugation at 400g for 5 minutes at room temperature, and the labeled cells were subjected to CytoFLEX flow cytometer (Beckman Coulter). A minimum of 20,000 events was acquired per sample. The cell death rate of the monocytes was analyzed by CytoFLEX flow cytometer with CytExpert software (Beckman Coulter). Monocytes were plated in 12-well plates at 300,000 cells per well and incubated in macrophage differentiation media for 24 hours (day1). After the incubation, suspended cells were collected by centrifugation (400g at 18°C for 5 minutes), and the remaining adherent cells were trypsinized at 37°C for 10 minutes. The suspended cells and adherent cells were combined and labeled with the EthD-1. The percentage of dead monocytes per each individual sample was measured by the flow cytometer.

Statistics. Results are expressed as mean \pm SD or percentage as appropriate. Comparisons between groups were made by using a nonparametric Mann-Whitney *U* test. $P < 0.05$ was considered significant. All analyses were performed using the GraphPad Prism 8.1.0 (GraphPad software) software package.

Study approval. Prior to study participation, all outpatient volunteers provided informed consent. The study protocol was reviewed and approved by University of Florida (Gainesville) IRB (protocol 2015-01051).

Author contributions

JL and MB designed the study, planned the experimental work, and analyzed the data. JL, NM, YL, KH, and KK performed experimental work and analyzed the data. JL and MB wrote the manuscript. NM, YL, KK, and KH critically reviewed the manuscript. All authors approved the submission of this manuscript.

Acknowledgments

We gratefully acknowledge Center for Bio-Medical Engineering Core Facility at Dankook University for providing equipment including computing resources. This study was supported by University of Florida Departmental funds (UF project no. 00045513 [MLB] and the Alpha1 Foundation Research Professorship [MLB]).

Address correspondence to: Mark Brantly, University of Florida College of Medicine, 1600 SW Archer Rd Rm M331, JHMHC PO Box 100225, Gainesville, Florida 32610, USA. Phone: 352.294.5117; Email: mbrantly@ufl.edu.

1. Korkmaz B, et al. Inhibition of neutrophil elastase by alpha1-protease inhibitor at the surface of human polymorphonuclear neutrophils. *J Immunol.* 2005;175(5):3329–3338.
2. Van't Wout EFA, et al. α 1-Antitrypsin production by proinflammatory and antiinflammatory macrophages and dendritic cells. *Am J Resp Cell Mol.* 2012;46(5):607–613.
3. Jonigk D, et al. Anti-inflammatory and immunomodulatory properties of α 1-antitrypsin without inhibition of elastase. *Proc Natl Acad Sci U S A.* 2013;110(37):15007–15012.
4. Zhou T, et al. Alpha-1 antitrypsin attenuates M1 microglia-mediated neuroinflammation in retinal degeneration. *Front Immunol.* 2018;9:1202.
5. Kueppers F, et al. Protein modeling to assess the pathogenicity of rare variants of SERPINA1 in patients suspected of having alpha 1 antitrypsin deficiency. *BMC Med Genet.* 2019;20(1):125.
6. Henaou MP, Craig TJ. Understanding alpha-1 antitrypsin deficiency: a review with an allergist's outlook. *Allergy Asthma Proc.* 2017;38(2):98–107.
7. Janciauskiene SM, et al. The discovery of α 1-antitrypsin and its role in health and disease. *Respir Med.* 2011;105(8):1129–1139.
8. Greene CM, McElvaney NG. Z α -1 antitrypsin deficiency and the endoplasmic reticulum stress response. *World J Gastrointest*

- Pharmacol Ther.* 2010;1(5):94–101.
9. Torres-Duran M, et al. Alpha-1 antitrypsin deficiency: outstanding questions and future directions. *Orphanet J Rare Dis.* 2018;13(1):114.
 10. Dunlea DM, et al. The impact of alpha-1 antitrypsin augmentation therapy on neutrophil-driven respiratory disease in deficient individuals. *J Inflamm Res.* 2018;11:123–134.
 11. Tubio-Perez RA, et al. Alpha-1 antitrypsin deficiency and risk of lung cancer: a systematic review. *Transl Oncol.* 2021;14(1):100914.
 12. Teckman JH, et al. The proteasome participates in degradation of mutant alpha 1-antitrypsin Z in the endoplasmic reticulum of hepatoma-derived hepatocytes. *J Biol Chem.* 2001;276(48):44865–44872.
 13. Tanash HA, Piitulainen E. Liver disease in adults with severe alpha-1-antitrypsin deficiency. *J Gastroenterol.* 2019;54(6):541–548.
 14. Stoller JK, Aboussouan LS. A review of α 1-antitrypsin deficiency. *Am J Resp Crit Care.* 2012;185(3):246–259.
 15. Hurley K, et al. Alpha-1 antitrypsin augmentation therapy corrects accelerated neutrophil apoptosis in deficient individuals. *J Immunol.* 2014;193(8):3978–3991.
 16. Carroll TP, et al. Evidence for unfolded protein response activation in monocytes from individuals with alpha-1 antitrypsin deficiency. *J Immunol.* 2010;184(8):4538–4546.
 17. Bazzan E, et al. α ₁-Antitrypsin polymerizes in alveolar macrophages of smokers with and without α ₁-antitrypsin deficiency. *Chest.* 2018;154(3):607–616.
 18. Lee J, et al. Alpha 1 antitrypsin-deficient macrophages have impaired efferocytosis of apoptotic neutrophils. *Front Immunol.* 2020;11:574410.
 19. Hu G, et al. Vitamin D₃-vitamin D receptor axis suppresses pulmonary emphysema by maintaining alveolar macrophage homeostasis and function. *EBioMedicine.* 2019;45:563–577.
 20. Johnsen IB, et al. Toll-like receptor 3 associates with c-Src tyrosine kinase on endosomes to initiate antiviral signaling. *EMBO J.* 2006;25(14):3335–3346.
 21. Petes C, et al. The Toll for trafficking: Toll-like receptor 7 delivery to the endosome. *Front Immunol.* 2017;8:1075.
 22. Hung T, et al. The Ro60 autoantigen binds endogenous retroelements and regulates inflammatory gene expression. *Science.* 2015;350(6259):455–459.
 23. Mu X, et al. Endogenous retroelements and the host innate immune sensors. *Adv Immunol.* 2016;132:47–69.
 24. Zhang Z, et al. Toward a structural understanding of nucleic acid-sensing Toll-like receptors in the innate immune system. *FEBS Lett.* 2017;591(20):3167–3181.
 25. Michlewska S, et al. Macrophage phagocytosis of apoptotic neutrophils is critically regulated by the opposing actions of pro-inflammatory and anti-inflammatory agents: key role for TNF-alpha. *FASEB J.* 2009;23(3):844–854.
 26. Pacheco GV, et al. Expression of TLR-7, MyD88, NF-kB, and INF- α in B lymphocytes of Mayan women with systemic lupus erythematosus in Mexico. *Front Immunol.* 2016;7:22.
 27. Sawant KV, et al. Chemokine CXCL1 mediated neutrophil recruitment: role of glycosaminoglycan interactions. *Sci Rep.* 2016;6:33123.
 28. Disteldorf EM, et al. CXCL5 drives neutrophil recruitment in TH17-mediated GN. *J Am Soc Nephrol.* 2015;26(1):55–66.
 29. Loos T, et al. Citrullination of CXCL8 increases this chemokine's ability to mobilize neutrophils into the blood circulation. *Hematologica.* 2009;94(10):1346–1353.
 30. Lebreton F, et al. NLRP3 inflammasome is expressed and regulated in human islets. *Cell Death Dis.* 2018;9(7):726.
 31. Swanson KV, et al. The NLRP3 inflammasome: molecular activation and regulation to therapeutics. *Nat Rev Immunol.* 2019;19(8):477–489.
 32. Qiao Y, et al. TLR-induced NF- κ B activation regulates NLRP3 expression in murine macrophages. *FEBS Lett.* 2012;586(7):1022–1026.
 33. Janciauskiene S, et al. The multifaceted effects of alpha1-antitrypsin on neutrophil functions. *Front Pharmacol.* 2018;9:341.
 34. Heissmeyer V, et al. NF-kappaB p105 is a target of IkappaB kinases and controls signal induction of Bcl-3-p50 complexes. *EMBO J.* 1999;18(17):4766–4778.
 35. Sakurai H, et al. IkappaB kinases phosphorylate NF-kappaB p65 subunit on serine 536 in the transactivation domain. *J Biol Chem.* 1999;274(43):30353–30356.
 36. Han K, et al. Under the genomic radar: the stealth model of Alu amplification. *Genome Res.* 2005;15(5):655–664.
 37. Maeda K, Akira S. TLR7 structure: cut in Z-loop. *Immunity.* 2016;45(4):705–707.
 38. Li TH, Schmid CW. Differential stress induction of individual Alu loci: implications for transcription and retrotransposition. *Gene.* 2001;276(1–2):135–141.
 39. Zhang ZK, et al. Structural analyses of Toll-like receptor 7 reveal detailed RNA sequence specificity and recognition mechanism of agonistic ligands. *Cell Rep.* 2018;25(12):3371–3381.
 40. Kim S, et al. Structural variation of Alu element and human disease. *Genomics Inform.* 2016;14(3):70–77.
 41. Bashir A, et al. Novel variants of SERPIN1A gene: interplay between alpha1-antitrypsin deficiency and chronic obstructive pulmonary disease. *Respir Med.* 2016;117:139–149.
 42. Bergin DA, et al. α -1 Antitrypsin regulates human neutrophil chemotaxis induced by soluble immune complexes and IL-8. *J Clin Invest.* 2010;120(12):4236–4250.
 43. Varfolomeev EE, Ashkenazi A. Tumor necrosis factor: an apoptosis JuNKie? *Cell.* 2004;116(4):491–497.
 44. Lawless MW, et al. Activation of endoplasmic reticulum-specific stress responses associated with the conformational disease Z alpha 1-antitrypsin deficiency. *J Immunol.* 2004;172(9):5722–5726.
 45. Alam S, et al. Z α 1-antitrypsin confers a proinflammatory phenotype that contributes to chronic obstructive pulmonary disease. *Am J Resp Crit Care.* 2014;189(8):909–931.
 46. Ozaki E, et al. Targeting the NLRP3 inflammasome in chronic inflammatory diseases: current perspectives. *J Inflamm Res.* 2015;8:15–27.
 47. Kelley N, et al. The NLRP3 inflammasome: an overview of mechanisms of activation and regulation. *Int J Mol Sci.* 2019;20(13):3328.

48. Faner R, et al. The inflammasome pathway in stable COPD and acute exacerbations. *ERJ Open Res.* 2016;2(3):00002-2016.
49. McElvaney OF, et al. Anti-cytokines as a strategy in alpha-1 antitrypsin deficiency. *Chronic Obstr Pulm Dis.* 2020;7(3):203–213.
50. Reed JH, Gordon TP. Autoimmunity: Ro60-associated RNA takes its toll on disease pathogenesis. *Nat Rev Rheumatol.* 2016;12(3):136–138.
51. Janciauskiene S, et al. Potential roles of acute phase proteins in cancer: why do cancer cells produce or take up exogenous acute phase protein alpha1-antitrypsin? *Front Oncol.* 2021;11:622076.
52. Teckman JH, Perlmutter DH. Retention of mutant alpha(1)-antitrypsin Z in endoplasmic reticulum is associated with an autophagic response. *Am J Physiol Gastrointest Liver Physiol.* 2000;279(5):G961–G974.
53. Wood AM, Stockley RA. Alpha one antitrypsin deficiency: from gene to treatment. *Respiration.* 2007;74(5):481–492.
54. Li H, Durbin R. Fast and accurate short read alignment with Burrows-Wheeler transform. *Bioinformatics.* 2009;25(14):1754–1760.
55. Liao Y, et al. featureCounts: an efficient general purpose program for assigning sequence reads to genomic features. *Bioinformatics.* 2014;30(7):923–930.